Physics of Fluids

RESEARCH ARTICLE | JUNE 23 2023

Why the reciprocal two-sphere swimmer moves in a viscoelastic environment FREE

Marcel Eberhard ; Akash Choudhary ; Holger Stark

Physics of Fluids 35, 063119 (2023)
https://doi.org/10.1063/5.0151585

AIP Publishing

Physics of Fluids ARTICLE pubs.aip.org/aip/pof

Why the reciprocal two-sphere swimmer moves in a viscoelastic environment

Cite as: Phys. Fluids **35**, 063119 (2023); doi: 10.1063/5.0151585
Submitted: 23 March 2023 · Accepted: 6 June 2023 ·
Published Online: 23 June 2023

View Online Export Citation CrossMark

Marcel Eberhard,[1,a)] Akash Choudhary,[1,2,b)] and Holger Stark[1,c)]

AFFILIATIONS

[1]Institute of Theoretical Physics, Technische Universität Berlin, Hardenbergstr. 36, 10623 Berlin, Germany
[2]Department of Chemical Engineering, Indian Institute of Technology Kanpur, Kanpur 208016, India

[a)]Author to whom correspondence should be addressed: eberhard@campus.tu-berlin.de
[b)]achoudhary@iitk.ac.in
[c)]holger.stark@tu-berlin.de

ABSTRACT

In Newtonian fluids, microswimmers need to perform a non-reciprocal shape change to move forward. However, this is no longer required in biological fluids with their viscoelastic properties. In this work, we investigate an oscillating two-sphere swimmer in a weakly viscoelastic fluid and show that the swimmer moves toward the smaller sphere. We use the flow fields generated by the individual spheres. Since they contain a viscoelastic contribution quadratic in the sphere velocities, the forces needed to expand and contract the swimmer differ from each other. This causes a non-zero net displacement during one cycle. We also find that the mean flow field generated by the two-sphere swimmer is the one of a contractile force dipole.

I. INTRODUCTION

The locomotion of micrometer-sized motile organisms is governed by low-Reynolds-number hydrodynamics, where viscous forces dominate inertia so that it is negligible.[1–3] For Newtonian fluids, the well-known scallop theorem introduced by Purcell[4] states that for microswimmers, undergoing a sequence of reciprocal periodic shape changes, the net displacement is zero. Here, reciprocal means that under time reversal, the periodic shape changes look the same. Hence, a microscopic scallop with only one hinge cannot swim by opening and closing, even if these two parts of a cyclic stroke are carried out at different speeds. Similarly, a simple model swimmer consisting of two spheres connected by a rod cannot swim by expanding and contracting, as the deformations are reciprocal in time. Numerous studies in the past have addressed biological and artificial microswimmers that employ a wide variety of propulsion mechanisms with non-reciprocal stroke patterns as documented, for example, by Refs. 1, 2, and 5–11. These investigations range from flagellated pathogens[5–9] to artificial swimmers using superparamagnetic filaments.[10,11]

In contrast to the sophisticated propulsion mechanisms of real microswimmers, simple models using linked spheres have the advantage that one can treat them analytically and thereby reveal the hydrodynamics of locomotion. One of the simplest models for a self-propelling microswimmer with a non-reciprocal stroke is the three-sphere swimmer introduced by Najafi and Golestanian.[12] It performs a net displacement provided the rods connecting the three spheres do not oscillate in phase. The alternative push-me-pull-you swimmer was introduced by Avron *et al.*[13] This two-sphere swimmer moves because the spheres exchange volume, while their distance oscillates. In either case, both swimmers use the minimal number of two degrees of freedom to break the time-reversal symmetry and further studies have optimized their design and stroke patterns.[14,15]

Microorganisms typically move in an environment governed by non-Newtonian fluids, such as sperm cells in the Fallopian tubes,[16] pathogens in lung mucus,[17] or bacteria in biofilms.[18,19] Furthermore, artificial swimmers with potential biomedical applications would also move in such environments.[20,21] Thus, understanding locomotion in non-Newtonian fluids is essential for designing functional nano-/micro-swimmers. This article aims to contribute to such an understanding by studying a reciprocal two-sphere swimmer in a weakly viscoelastic fluid.

The properties of non-Newtonian fluids can, on the one hand, modify the motion of non-reciprocal microswimmers[22–30] and, on the other hand, overcome the scallop theorem to enable locomotion by reciprocal deformations.[31] Curtis and Gaffney[24] showed that the Najafi–Golestanian swimmer moves faster and with a higher efficiency in viscoelastic fluids, while for spherical squirmers, which are driven

by surface velocities fields, swimming is either improved or impeded.[25] Furthermore, non-linear viscoelasticity can also enable squirmers to swim, which would otherwise not show locomotion in Newtonian fluids.[32] Qiu *et al.*[33] and Han *et al.*[34] demonstrated directed motion of a micro-scallop in shear-thinning and shear-thickening fluids. The propulsion mechanism of the "snowman" swimmer relies on normal stress differences,[35] and the predicted locomotion was experimentally verified by Puente-Velázquez *et al.*[36] Inspired by this, Binagia and Shaqfeh[37] and Kroo *et al.*[38] recently designed and studied a torque-free "snowman" swimmer that had an internal rotation mechanism. Most importantly, in contrast to Newtonian fluids, an oscillating two-sphere swimmer with only one degree of freedom is able to move forward in a viscoelastic fluid. Using domain perturbation expansion[32] and the reciprocal theorem, Datt *et al.*[39] calculated the average swimming velocity of such a two-sphere swimmer in an Oldroyd-B fluid for small oscillation amplitudes and arbitrary Deborah number. Yasuda *et al.*[40] also investigated the two-sphere swimmer and extended the analysis for a general linear viscoelastic fluid. An experimental study by Keim *et al.*[41] designed a proof-of-concept dimer with a different propulsion mechanism. They showed that reciprocal oscillations of the dimer's orientation in an external magnetic field enable targeted locomotion. All of these studies showed that structural asymmetry of the swimmer is essential for breaking the symmetry.

In this article, we investigate the two-sphere swimmer in a weakly viscoelastic fluid for arbitrary oscillation amplitude and demonstrate the underlying mechanisms for self-propulsion as well as the generated flow field in the ambient fluid. We employ the flow field of a dragged sphere derived by Housiadas and Tanner[42] for the Phan–Thien–Tanner (PTT) fluid. We calculate the forces experienced by the two spheres of the swimmer, its swimming velocity, and its net displacement. We show that locomotion only is possible when the two spheres have different sizes. Furthermore, we describe the swimmer kinematics in detail and discuss how swimming depends on the geometry of the swimmer. Finally, we derive the time-averaged flow field far from the swimmer using a similar approach as Alexander *et al.*[43] and find that the swimmer generates the long-range flow field of a contractile hydrodynamic dipole.

In Sec. II, we introduce the two-sphere model swimmer and the flow field of a single dragged sphere in a weakly viscoelastic fluid, which we use to analyze the model swimmer. Section III contains the results and discusses the two-sphere swimmer in detail. Finally, we conclude in Sec. IV.

II. MODEL SWIMMER AND FLOW FIELDS

Figure 1 shows the schematic of the swimmer investigated in this work. It consists of two spheres with radii $a_1 = a$ and $a_2 = a/\alpha$, where $\alpha = a_1/a_2$ is the sphere size ratio, and we assume $\alpha > 1$ without loss of generality. The spheres are connected by an infinitesimally thin rod that changes its length according to

$$\tilde{L}(t) = \tilde{L}_0 - \tilde{d}_0 \cos(\omega \tilde{t}). \tag{1}$$

Here, $\tilde{L}_0$ is the average distance between the spheres, $\tilde{d}_0$ is the oscillation amplitude, ω is the oscillation frequency, and tilde indicates dimensional variables. The neutrally buoyant swimmer is freely suspended and thus satisfies the force-free condition,

$$\tilde{f}_1 + \tilde{f}_2 = 0, \tag{2}$$

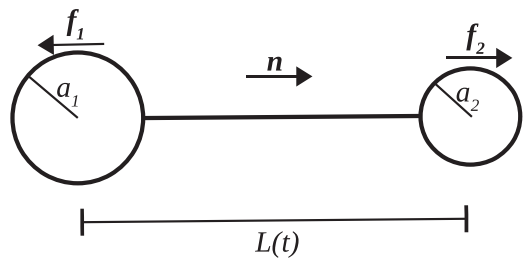

FIG. 1. Schematic of the two-sphere swimmer with spheres of radii $a_1 = a$ and $a_2 = a/\alpha$ that are connected by a rod of length $L(t)$. The unit vector $\boldsymbol{n}$ points along the swimmer in direction of the smaller sphere. $f_1\boldsymbol{n}$ and $f_2\boldsymbol{n}$ are the forces exerted by the rod on spheres 1 and 2. Throughout the article, all lengths are given in units of $a_1 = a$.

where $\tilde{f}_1$ and $\tilde{f}_2$ are the forces exerted by the rod on spheres 1 and 2, respectively.

Our calculations utilize the flow field derived by Housiadas and Tanner[42] for a single sphere moving with constant velocity in a viscoelastic fluid, which is modeled with the Phan–Thien–Tanner (PTT) constitutive equation. The fluid is further characterized by the relaxation time λ and the shear viscosity $\tilde{\eta} = \tilde{\eta}_s + \tilde{\eta}_p$ that consists of a solvent and a polymer contribution.

In the following, we switch to non-dimensional quantities. In viscoelastic fluids, the total stress tensor $\mathbf{S}$ consists of the Newtonian stress, $-p\mathbf{I} + \eta_s\dot{\gamma}$, and the polymeric stress quantified by $\boldsymbol{\sigma}_p$. Here, p is the pressure, $\dot{\gamma}$ is the rate-of-strain tensor, and $\eta_s = \frac{\tilde{\eta}_s}{\tilde{\eta}}$ represents the solvent-to-total viscosity ratio. The PTT constitutive equation determines $\boldsymbol{\sigma}_p$ as

$$\sigma_p \exp(\epsilon \mathrm{De}\, \mathrm{tr}\sigma_p) + \mathrm{De}\, \overset{\nabla}{\sigma}_p = \dot{\gamma}. \tag{3}$$

Here, $\mathrm{tr}(\cdot)$ is the trace operator, and the upper convected derivative is defined as $\overset{\nabla}{\boldsymbol{\sigma}}_p := \boldsymbol{u} \cdot \nabla \boldsymbol{\sigma}_p - \boldsymbol{\sigma}_p \cdot \nabla \boldsymbol{u} - (\nabla \boldsymbol{u})^T \cdot \boldsymbol{\sigma}_p$, where $\boldsymbol{u}$ is the velocity of the flow field. Furthermore, $\mathrm{De} = \lambda\omega$ is the Deborah number, where λ is the polymer relaxation time, and ω is the imposed oscillation frequency. The dimensionless material parameter ϵ introduces a nonlinearity in $\boldsymbol{\sigma}_p$, and for $\epsilon = 0$, Eq. (3) becomes identical to the Oldroyd-B constitutive equation. By solving the incompressibility condition, $\nabla \cdot \boldsymbol{u} = 0$, and the momentum balance, $\nabla \cdot \mathbf{S} = 0$, perturbatively in De, Housiadas and Tanner[42] obtained the flow field of a sphere moving with velocity v_n. To leading order in De and up to terms of $1/r^2$, its non-dimensional form is given by[44]

$$\boldsymbol{u}_n(\boldsymbol{r}) = \frac{3}{4}\frac{a_n v_n}{r}\left[\boldsymbol{n} + (\hat{\boldsymbol{r}} \cdot \boldsymbol{n})\hat{\boldsymbol{r}}\right] - \frac{3}{8}\mathrm{De}\, \eta_p \frac{a_n v_n^2}{r^2}\left[-1 + 3(\hat{\boldsymbol{r}} \cdot \boldsymbol{n})^2\right]\hat{\boldsymbol{r}} \tag{4}$$

with $n \in \{1, 2\}$, $\hat{\boldsymbol{r}} = (\boldsymbol{r} - \boldsymbol{r}_n)/r$, $r = |\boldsymbol{r} - \boldsymbol{r}_n|$, and $\boldsymbol{r}_n$ as the position of each sphere. Furthermore, $\eta_p = \frac{\tilde{\eta}_p}{\tilde{\eta}}$ represents the polymer-to-total viscosity ratio, and, in the following, we assume the Deborah number De to be small ($\mathrm{De} \ll 1$). The flow fields $\boldsymbol{u}_n$ and the sphere velocities v_n are scaled with $a\omega$, the distance r and sphere sizes with a such that the respective radii are $a_1 = 1$ and $a_2 = 1/\alpha$. Note that, at this order of approximation (up to terms linear in De), the flow field does not depend on the parameter ϵ. Thus, to linear order in De, the PTT and the Oldroyd-B model give the same results.

In the following, we perform a perturbation analysis up to first order in De. Since in this order, the drag coefficient is the same as in the Newtonian limit,[42] we replace the particle velocities v_n in Eq. (4) by their Stokes drag forces $f_n = v_n \alpha^{1-n}$ written in units of $6\pi\tilde{\eta}a^2\omega$ and obtain

$$\boldsymbol{u}_n(\boldsymbol{r}) = \frac{3}{4}\frac{f_n}{r}[\boldsymbol{n} + (\hat{\boldsymbol{r}}\cdot\boldsymbol{n})\hat{\boldsymbol{r}}] - \frac{3}{8}\mathrm{De}\,\eta_p\frac{f_n^2\alpha^{n-1}}{r^2}\left[-1 + 3(\hat{\boldsymbol{r}}\cdot\boldsymbol{n})^2\right]\hat{\boldsymbol{r}}. \quad (5)$$

The flow field consists of two components at this order of approximation. The first term is the conventional Stokeslet: the far-field hydrodynamic signature of a forced sphere in a Newtonian fluid, which decays as $1/r$. The second term is a modification that arrives from the viscoelastic PTT fluid, which is equivalent to the flow field of a contractile force dipole that decays as $1/r^2$. In contrast to the Stokeslet, the strength of the dipole field depends on the size of the sphere via the factor α^{n-1} and quadratically on the force f_n driving the motion. The dependence on f_n^2 introduces a fore-aft asymmetry that we describe now. In a Newtonian fluid, the flow field of a Stokeslet is antisymmetric with respect to a plane perpendicular to the point force. As the symmetric force-dipole field is added, the flow field becomes asymmetric: The strength of the flow field is higher at the rear than in front of the moving sphere. This is because the Stokeslet and the force-dipole fields point in the same direction behind the sphere but in opposite directions in front of it. This asymmetry eventually is responsible for the net movement of our swimmer when averaged over one cycle of its reciprocal deformation.

Now, the sphere n within our swimmer is moved by the force f_n acting on it, but also advected by the flow field generated by the neighboring sphere as described by Eq. (5). Thus, assuming $L \gg a$, we can write the velocities of both spheres as[45–47]

$$v_1 = f_1 + \frac{3f_2}{2L} + \frac{3}{4}\mathrm{De}\,\eta_p\frac{\alpha f_2^2}{L^2}, \quad (6a)$$

$$v_2 = \alpha f_2 + \frac{3f_1}{2L} - \frac{3}{4}\mathrm{De}\,\eta_p\frac{f_1^2}{L^2}, \quad (6b)$$

where $L = L_0 - d_0\cos(t)$ is the non-dimensionalized arm length with $L_0 = \tilde{L}_0/a$, $d_0 = \tilde{d}_0/a$ and $t = \omega\tilde{t}$. The first term on the right-hand side is caused by the driving of the oscillation, and α^{1-n} is the Stokes drag coefficient of sphere n in our dimensionless units. The remaining terms represent the advection in the flow field of the other sphere. Since the prescribed arm length $L(t)$ is the distance between both spheres, their velocities are connected by

$$\dot{L} = v_2 - v_1. \quad (7)$$

Thus, we have a set of four equations, Eqs. (2), (6a), (6b), and (7), for the four unknown quantities v_1, v_2, f_1, and f_2. Solving these equations gives the quantities as functions of L and $\dot{L}$.

III. RESULTS AND DISCUSSION

In the following, we present the results of our investigations. First, we show that viscoelasticity breaks the symmetry between expansion and contraction during one cycle by studying the force component solely due to viscoelasticity (Sec. III A). Second, we calculate the net displacement of the swimmer and investigate how the ability to swim depends on the size ratio of the two swimmer spheres (Sec. III B). Finally, we show that the swimmer generates the long-range flow field of a contractile force dipole (Sec. III C).

A. Mechanics of deformation

As a first step of solving our set of equations, we use the force-free condition, Eq. (2), to introduce $f := f_1 = -f_2$ and eliminate one of the forces in Eq. (6). By using Eqs. (6) and (7), we obtain a quadratic equation for the force f. Discarding an unphysical solution, the relevant solution to leading order in De is given by the following equation:

$$\begin{aligned} f &= f^N + \mathrm{De}\,f^{VE} \\ &= -\frac{\dot{L}}{\alpha + 1 - 3/L}\left(1 + \frac{3}{4}\mathrm{De}\,\frac{\eta_p(\alpha+1)\dot{L}}{[L(\alpha+1)-3]^2}\right). \end{aligned} \quad (8)$$

Thus, the force experienced by sphere 1 is separated into a Newtonian (f^N) and a viscoelastic ($\mathrm{De}\,f^{VE}$) component. In Fig. 2(a), we compare the acting forces in a Newtonian and a viscoelastic fluid. We first consider the simplest case of non-interacting spheres ($L \to \infty$), where one has just the Stokes drag of the Newtonian fluid, which gives $f = f^{\mathrm{non}} = -\dot{L}/(\alpha+1)$ [black dotted line in Fig. 2(a)]. At $t = 0$, the swimmer is in a fully contracted state. Then, it expands with velocity $\dot{L}(t)$, which requires a negative force to move sphere 1 to the left. The swimmer achieves full expansion at $t = \pi$, followed by a contraction toward the original state at $t = 2\pi$. The forces needed to expand and contract the swimmer are identical in magnitude as the asymmetry of the black dotted curve about $t = \pi$ shows. The minimum and maximum are exactly at the maximum speeds of actuation at $t = \pi/2$ and $3\pi/2$, respectively. The orange dashed curve shows the full Newtonian component f^N with the far-field hydrodynamic interactions between the spheres included. Clearly, the advection from the neighboring sphere increases the magnitude of the acting force since the advection velocity from sphere 2 always acts against expansion or contraction. This can be also checked from Eq. (6a), where f_1 and $f_2 = -f_1$ have

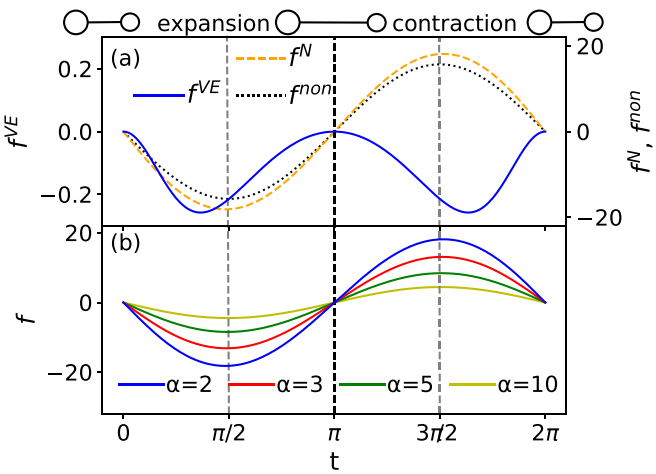

FIG. 2. (a) Forces acting on sphere 1 plotted vs time for one cycle period with expansion and contraction. Non-interacting spheres: f^{non} (black dotted line), Newtonian component f^N (orange dashed line), and viscoelastic component f^{VE} (blue solid line). The schematics on top of the graph indicate the swimmer configuration at times $t = 0$, π, and 2π, respectively. (b) Total force f for different size ratios. Parameters are $\mathrm{De} = 0.1$, $\eta_p = 0.8$, $L_0 = 7.5$, $d_0 = 2.5$, and $\alpha = 2$.

always opposite signs. However, since L varies in time, its minimum and maximum are slightly shifted toward the fully contracted rod at $t = 0$ and 2π.

In a viscoelastic fluid, the symmetry across the two halves of cycle, expansion and contraction, is broken. The blue curve in Fig. 2(a) shows the viscoelastic force component $\mathrm{De} f^{VE}$ acting on sphere 1. When the swimmer extends, it now requires a larger negative force as represented by the negative contribution f^{VE}. This is because the contractile force-dipole flow field due to viscoelasticity [last term in Eq. (6a)] acts against expansion. However, it supports contraction, which results in a smaller total force due to $f^{VE} < 0$. In Eq. (8), all this behavior is manifested by the different dependence on $\dot{L}$ in f^N and f^{VE}. The Newtonian force is linear in $\dot{L}$, whereas the viscoelastic component is quadratic in $\dot{L}$. Thus, while f^N changes sign when switching from expansion to contraction, f^{VE} does not. Furthermore, we note that the minima of f^{VE} are further shifted toward the contracted state. This is also suggested by Eq. (8), since f^{VE} strongly depends on L and not just $\dot{L}$.

We also show the effect of increasing size ratio on the total force during actuation in Fig. 2(b). As suggested by the appearance of α in the denominator of the prefactor in Eq. (8), the magnitude of the force decreases because the larger sphere 1 hardly moves due to its larger friction and, conversely, the smaller sphere 2 would oscillate without needing much force.

B. Swimming kinematics

By substituting the force from Eq. (8) back in the relations of Eq. (6), the velocities of the individual spheres are obtained. Upon taking the arithmetic mean of these velocities, $V = (v_1 + v_2)/2$, we obtain the velocity of the center of the swimmer, which we name its instantaneous swimming velocity V. To leading order in De, it is given by

$$\begin{aligned} V &= V^N + \mathrm{De}\, V^{VE} \\ &= \frac{\alpha - 1}{2} \frac{\dot{L}}{\alpha + 1 - 3/L} \left(1 + \frac{3}{4} \mathrm{De}\, \eta_p \frac{\dot{L}}{L} \frac{2L(\alpha+1) - 3}{(L(\alpha+1) - 3)^2} \right). \end{aligned} \tag{9}$$

By integrating the velocity over time, we obtain the instantaneous position of the swimmer with respect to the initial position of its center (origin),

$$R(t) = \int_0^t V dt' = R^N(t) + \mathrm{De}\, R^{VE}(t). \tag{10}$$

With this, we can now conveniently obtain the positions of the single spheres by subtracting and adding half of the oscillating arm length,

$$r_1(t) = R(t) - \frac{L(t)}{2}, \quad r_2(t) = R(t) + \frac{L(t)}{2}. \tag{11}$$

Evaluating the integral in Eq. (10) gives an analytical expression for the position of the swimmer.

The Newtonian contribution in Eq. (10) is given by

$$R^N(t) = \frac{\alpha - 1}{\alpha + 1} \left[\frac{d_0}{2} (1 - \cos(t)) - \frac{1}{2} \frac{3}{\alpha + 1} \ln \left(\frac{l_0 - d_0}{l_0 - d_0 \cos(t)} \right) \right], \tag{12}$$

with $l_0 = L_0 - \frac{3}{\alpha+1}$. After one full time period, it is zero, as expected from the scallop theorem. For the viscoelastic contribution, we obtain

$$\begin{aligned} \mathrm{De} R^{VE}(t) = \frac{3}{16} \frac{\alpha - 1}{(\alpha+1)^2} \mathrm{De}\, \eta_p \Bigg(-4t - \frac{3}{\alpha+1} \frac{\dot{L}}{(3/(\alpha+1) - L)^2} \\ - \frac{\dot{L}}{(3/(\alpha+1) - L)} \\ \times \frac{\left[4(L_0^2 - d_0^2) + 45/(\alpha+1)^2 - 27 L_0/(\alpha+1) \right]}{(l_0^2 - d_0^2)} \\ + \frac{8 l_0^3 - 2 d_0^2 [4 l_0 - 3/(\alpha+1)]}{(l_0^2 - d_0^2)^{3/2}} G(t) \Bigg), \end{aligned} \tag{13}$$

where we have defined

$$G(t) = \begin{cases} \arctan\left(\frac{l_0 + d_0}{\sqrt{l_0^2 - d_0^2}} \tan\left(\frac{t}{2} \right) \right) & 0 < t < \pi \\ \arctan\left(\frac{l_0 + d_0}{\sqrt{l_0^2 - d_0^2}} \tan\left(\frac{t}{2} \right) \right) + \pi & \pi < t < 2\pi. \end{cases} \tag{14}$$

In Fig. 3(a), the positions of the swimmer and the two spheres are shown. The swimmer moves forward (toward the smaller sphere) during expansion and backward during contraction. This back and forth motion covers a much larger distance than the total displacement after one swimming stroke. As the size ratio is raised (red dashed line), the distance covered by the smaller sphere increases, whereas the larger sphere moves less. As a result, for the half-cycle of expansion,

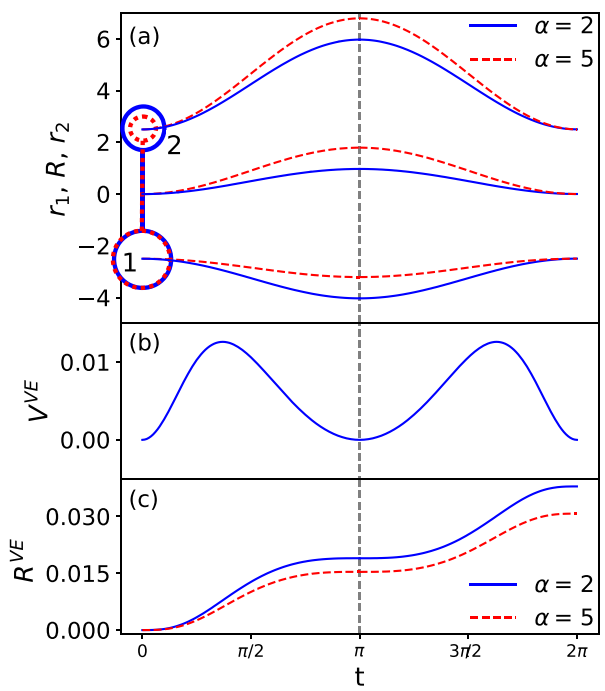

FIG. 3. (a) Positions of the swimmer (middle trajectory) and spheres 1 and 2 during one swimming stroke for two size ratios α. (b) Viscoelastic component V^{VE} of the velocities of spheres 1 and 2 for $\alpha = 2$. (c) Swimmer displacement $R^{VE}(t)$ due to viscoelasticity for two size ratios α. Other parameters are $\mathrm{De} = 0.1$, $\eta_p = 0.8$, $L_0 = 7.5$, and $d_0 = 2.5$.

the increasing size ratio always increases displacement. However, for the full cycle, there is an optimum size ratio (as will later be shown in Fig. 4). The viscoelastic velocity component is the same for both spheres, since one immediately derives from Eq. (11) and $v_n = \dot{r}_n(t)$ that $\mathrm{De} v_n^{VE} = v_n - v_n^N = \mathrm{De} V^{VE}$. We show V^{VE} in Fig. 3(b) and discuss the consequences. Since always $V^{VE} > 0$, we immediately recognize that during expansion the larger sphere is slower and the smaller sphere faster compared to a Newtonian fluid. Thus, the swimmer moves a larger distance in the first half cycle, as shown in Fig. 3(c), where we plot the viscoelastic contribution to the displacement, $R^{VE}(t)$. During contraction, the first sphere is faster and the second one slower than in a Newtonian fluid. Again, this gives a positive displacement $R^{VE}(t)$. So, in a sum the swimmer in a viscoelastic environment moves forward with a net displacement after one swimming stroke. At larger size ratios (red dashed line), the displacement becomes smaller, as discussed further below.

We now analyze the net displacement after one swimming stroke by evaluating the position of the swimmer at $t = 2\pi$,

$$\begin{aligned} R(2\pi) &= \mathrm{De}\, R^{VE}(2\pi) \\ &= \frac{3}{8}\mathrm{De}\,\eta_p \pi \frac{\alpha - 1}{(\alpha+1)^2}\left(l_0^2 - d_0^2\right)^{-3/2} \\ &\quad \times \left[4 l_0^2\left(l_0 - \sqrt{l_0^2 - d_0^2}\right) + d_0^2\left(\frac{3}{\alpha+1} - 4 l_0 + 4\sqrt{l_0^2 - d_0^2}\right)\right]. \end{aligned} \tag{15}$$

The Newtonian contribution to the total displacement vanishes $[R^N(2\pi) = 0]$. As already stated, this is expected from the scallop theorem.[4] Only the contribution due to viscoelasticity gives a net displacement after one swimming cycle.

To summarize our results so far, we find that the total displacement during one swimmer cycle is positive, i.e., the swimmer moves forward with the smaller sphere as the head. This was also shown previously by Datt *et al.*[39] via the reciprocal theorem. As our formulas also show, the size anisotropy is crucial for breaking the symmetry of the swimmer; for same-size spheres ($\alpha = 1$), the swimmer's center is at rest for all times. Increasing the size ratio from one enables the swimmer to move in a viscoelastic environment since after expansion, it does not completely return to the initial position during contraction. However, in the limit $\alpha \gg 1$, the net displacement of the swimmer should also approach zero. Sphere 1 has such a large friction coefficient so that it hardly moves, while the smaller sphere just oscillates about a mean position. This view is confirmed by Fig. 4, where we plot the total displacement from Eq. (15) vs α. There exists an ideal size ratio α_{max} where the maximum displacement is achieved. Increasing the average distance L_0 between the spheres reduces the net displacement due to the weaker hydrodynamic interactions (*c.f.* blue and red solid lines in Fig. 4). Decreasing the oscillation amplitude d_0 reduces the oscillation speed and thereby the total displacement (*c.f.* green solid line). Finally, in the inset, we demonstrate that the optimum size ratio α_{max} increases with increasing L_0, albeit slowly, and with decreasing d_0 due to reduced hydrodynamic interactions.

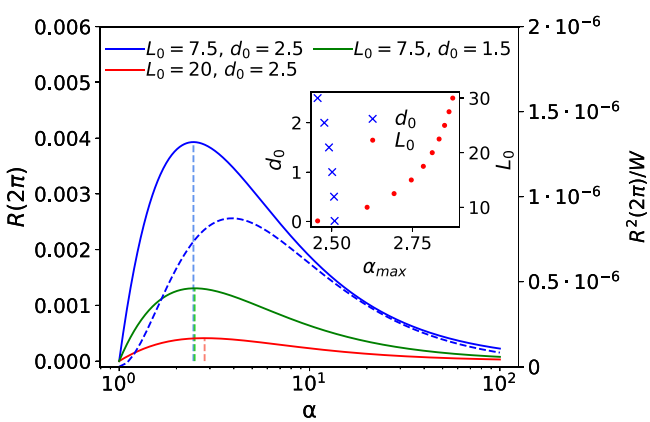

FIG. 4. Total displacement after one swimming stroke plotted vs sphere-size ratio α. Curves for different combinations L_0 and d_0 are shown. Dashed blue line: hydrodynamic efficiency $R^2(2\pi)/W$ plotted vs α. The same parameters as solid blue line. Inset: optimum size ratio α_{max} vs L_0 for $d_0 = 2.5$ and vs d_0 for $L_0 = 7.5$. Other parameters are $\mathrm{De} = 0.1$ and $\eta_p = 0.8$.

Microswimmers dissipate a lot of energy. So it seems to make sense to relate the total displacement to the total work done by the oscillating swimmer and find the optimal size ratio, which gives the largest displacement per unit work done. We therefore determine the total work $W = \int_0^{2\pi}(f_1 v_1 + f_2 v_2)dt$, which after some lengthy calculations becomes

$$W = -\int_0^{2\pi} f\dot{L}\, dt = \frac{\pi}{\alpha+1}\left(d_0^2 - \frac{6}{\alpha+1}\left[-l_0 + \sqrt{l_0^2 - d_0^2}\right]\right). \tag{16}$$

Interestingly, the optimal displacement per unit work, $R(2\pi)/W$, does not show a maximum when varying α but increases monotonically from zero and approaches a finite value for $\alpha \to \infty$.

Alternatively, one can look at the hydrodynamic efficiency introduced by Lighthill and examine $R^2(2\pi)/W$.[48] Since in our reduced units, $R(2\pi)/2\pi$ is the mean velocity of the swimmer, this ratio compares the energy dissipated by a swimmer moving constantly with velocity $R(2\pi)/2\pi$ to the actually dissipated energy up to a factor of $1/2\pi$. In Fig. 4, we plot $R^2(2\pi)/W$ vs α as dashed blue line for the same parameters as the solid blue line. Indeed, it has a maximum at $\alpha \approx 3.87$, which is larger than α value for the maximum of $R(2\pi)$.

Finally, we compare our findings to the work of Datt *et al.*[39] It has an overlapping regime of validity with our work for $\mathrm{De} \ll 1$ (our approximation) and $d_0 \ll 1$ (their approximation). Performing a Taylor expansion of $R(2\pi)$ up to leading order in the oscillation amplitude d_0, we find for the mean velocity in our reduced units,

$$\frac{R(2\pi)}{2\pi} \propto \eta_p \mathrm{De} \frac{d_0^2}{l_0^2}\frac{\alpha - 1}{(\alpha+1)^2}. \tag{17}$$

The linear dependence on De, η_p, d_0^2, and oscillation frequency ω (considering our rescaled time) agrees with Ref. 39. The dependence on l_0 and α is contained in a numerical factor in Ref. 39, but qualitatively, the decreasing velocity $R(2\pi)/2\pi$ with increasing swimmer length l_0 agrees with their findings.

C. Flow field

In addition to the net movement of the swimmer, cyclic deformations generate a time-averaged flow field. We are interested to determine its type since this type determines the nature of the swimmer being effectively a pusher, puller, or neutral. The corresponding flow

field is important for describing hydrodynamic interactions between the swimmers. To obtain the flow field, we first take the instantaneous flow field as a superposition of the flow fields of the two spheres,[43] which we already introduced in Eq. (5). We recognize that Eq. (5) can be rewritten in terms of the Oseen tensor $G_{ij}(\boldsymbol{r}-\boldsymbol{r}_n)$ and its derivative. Thus, we obtain[49]

$$u_i(\mathbf{r}) = \sum_{n=1}^{2}\left(\frac{3}{4}f_n G_{ij}(\mathbf{r}-\mathbf{r}_n)n_j + \frac{3}{8}\mathrm{De}\,\eta_p f_n^2 \alpha^{n-1} G_{ij,k}(\mathbf{r}-\mathbf{r}_n)n_j n_k\right), \tag{18}$$

where

$$G_{ij}(\boldsymbol{r}-\boldsymbol{r}_n) = \frac{1}{r}\left[\delta_{ij} + \hat{r}_i\hat{r}_j\right] \tag{19}$$

is the Oseen tensor, and

$$G_{ij,k}(\boldsymbol{r}-\boldsymbol{r}_n) = -\frac{1}{r^2}\left[\delta_{ij}\hat{r}_k - \delta_{ik}\hat{r}_j - \delta_{jk}\hat{r}_i - 3\hat{r}_i\hat{r}_j\hat{r}_k\right] \tag{20}$$

its derivative with respect to r_k. Furthermore, we used $\boldsymbol{f}_n = f_n\boldsymbol{n}$.

We obtain the time-averaged flow field by integrating the instantaneous flow field over one swimming stroke,

$$\bar{u}_i(\boldsymbol{r}) = \frac{1}{2\pi}\int_0^{2\pi} u_i(\boldsymbol{r})dt. \tag{21}$$

However, solving this integral is difficult because the positions of the spheres $\boldsymbol{r}_n(t)$ change over time, rendering the Oseen tensor time-dependent such that direct integration does not give any tractable analytical results. Thus, we seek a multipole expansion of the swimmer flow field around $\boldsymbol{r}$ to characterize it far from the swimmer position. With the initial position of the center of the swimmer at the origin, the position vectors of the single spheres are given by $\boldsymbol{r}_n = r_n(t)\boldsymbol{n}$. In the far field, we can now assume that the distance to the point of observation is large compared to the displacement of the spheres, i.e., $|\boldsymbol{r}| \gg |r_n(t)|$. Thus, we expand the Oseen tensor into a series in $1/r$,

$$G_{ij}(\boldsymbol{r}-\boldsymbol{r}_n) = \sum_{m=0}^{\infty}\frac{(-1)^m}{m!}G_{ij,k_1\cdots k_m}(\boldsymbol{r})n_{k_1}\cdots n_{k_m}r_n^m. \tag{22}$$

The expansion of its derivative is accordingly given by

$$G_{ij,k}(\boldsymbol{r}-\boldsymbol{r}_n)n_k = -\sum_{m=0}^{\infty}\frac{m(-1)^m}{m!}G_{ij,k_1\cdots k_m}(\boldsymbol{r})n_{k_1}\cdots n_{k_m}r_n^{m-1}. \tag{23}$$

By inserting this in Eqs. (18) and (21), we obtain the multipole expansion of the time-averaged flow field as

$$\bar{v}_i(\boldsymbol{r}) = \sum_{m=0}^{\infty}\frac{(-1)^m}{m!}G_{ij,k_1\cdots k_m}(\boldsymbol{r})n_{k_1}\cdots n_{k_m}\cdot \left[\frac{3}{8\pi}\int_0^{2\pi}\sum_{n=1}^{2}f_n r_n^m dt - \frac{3m\mathrm{De}\,\eta_p}{16\pi}\int_0^{2\pi}\sum_{n=1}^{2}\alpha^{n-1}f_n^2 r_n^{m-1}dt\right]. \tag{24}$$

This field consists of two factors: The first one (top row) describes how the flow field decays with distance and how it depends on relative position to the swimmer. The second factor (in squared brackets) is the strength of the respective multipole. It contains the moments of the forces acting on the swimmer ($\sum_{n=1}^{2} f_n r_n^m$) but also of the squared forces. Since from the beginning we only considered terms up to order $1/r^2$, to be consistent, we focus on the monopole and dipole term of this field. In the monopole term, only the Stokeslet of the total force contributes, which vanishes due to the force-free condition. Hence, the far field is dominated by a dipolar flow ($m = 1$). To evaluate the dipole strength, we use $f := f_1 = -f_2 = f^N + \mathrm{De}f^{VE}$ introduced in Eq. (8) and find to leading order in De,

$$p = p_1 + p_2 + p_3 = -\frac{3}{8\pi}\int_0^{2\pi} f^N L\,dt - \frac{3\mathrm{De}}{8\pi}\int_0^{2\pi} f^{VE}L\,dt - \frac{3\mathrm{De}\,\eta_p(\alpha+1)}{16\pi}\int_0^{2\pi}(f^N)^2\,dt. \tag{25}$$

The dipole consists of three terms: The first two are regular force-dipole strengths given by the product of force and distance with the force being split up into the Newtonian and viscoelastic part. The third term exists because a single sphere already exhibits a dipolar field.[42] When evaluating the integrals, one realizes that the first contribution has to vanish because the swimmer cycle is reciprocal and due to Stokes flow reversibility, a non-zero average flow field cannot arise in a Newtonian fluid by oscillating an object about a mean position. The second term gives a positive dipole moment since $f^{VE} \leq 0$. This means, as already discussed in Sec. III A, that the total force on each sphere is larger during the expansion than during the contraction. Thus, the net force acting on each sphere over one cycle points outward, indicating a pusher or extensile dipole. The last contribution to the dipole moment is negative and connected to the fact that the dipolar field of the individual sphere is contractile. Now, since the Newtonian force f^N is roughly two orders of magnitude larger than the viscoelastic force f^{VE} [see Fig. 2(a)], the third contribution is the largest and the dipolar flow field is governed by a negative total dipole strength [see Figs. 5(b) and 5(c)]. Thus, the swimmer generates a puller-like flow field as depicted in Fig. 5(a).

In Fig. 5(c), we plot the dipole strength vs the sphere-size ratio α for different combinations of (L_0, d_0). The dipole strength is the strongest for two spheres of the same size, although the swimmer does not exhibit any net displacement. Then, the magnitude of the total dipole moment decreases with increasing α since the magnitude of f^N scales with $1/\alpha$ as Eq. (8) shows. Increasing L_0 significantly only slightly reduces the dipole strength (solid blue and dotted red line) because the contribution of hydrodynamic interactions to f^N is minor compared to the direct force. However, reducing d_0 strongly decreases the dipole strength, as the actuation speed $\dot{L}$ and therefore the forces are reduced (green dashed line).

IV. CONCLUSIONS

Motivated by the abundance of examples of microbial motility in biological systems, the current work highlights the mechanics and flow field around a reciprocal two-sphere swimmer. For this purpose, we rely on the hydrodynamic flow field around a sphere that moves with constant velocity in viscoelastic fluid modeled by the PTT constitutive equation. The flow field was derived by Housiadas and Tanner,[42] and we use it in the limit of small De to describe the hydrodynamic interactions between both spheres that enable locomotion in the viscoelastic fluid.

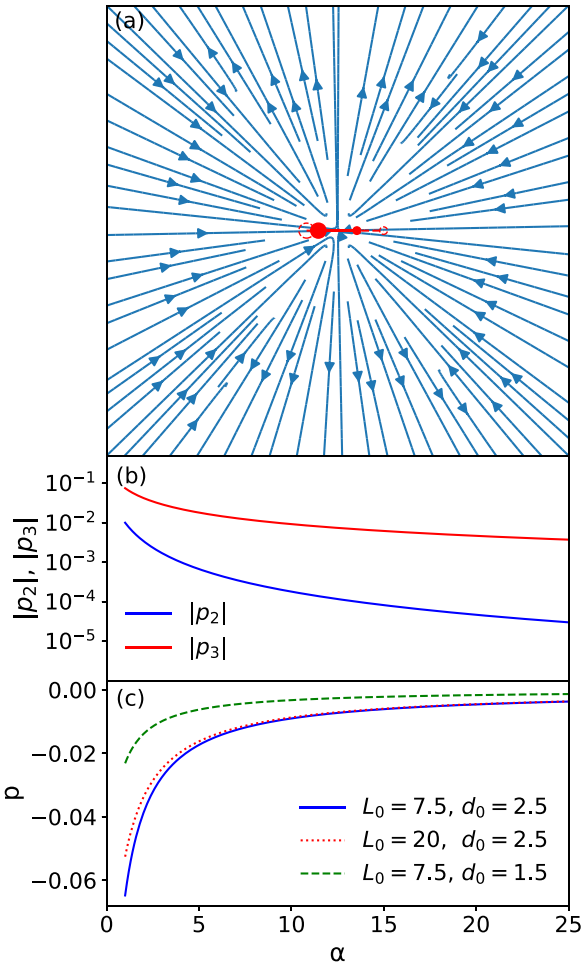

FIG. 5. (a) The two-sphere swimmer generates a time-averaged contractile dipolar flow field sufficiently far from the swimmer, for which we draw the streamlines. The size ratio is $\alpha = 2$. (b) Different contributions to the dipole strength in Eq. (25) plotted vs α. (c) Total dipole moment plotted vs α for different combinations of (L_0, d_0). Other parameters are De $= 0.1$, $\eta_p = 0.8$, $L_0 = 7.5$, and $d_0 = 2.5$, if not stated otherwise.

We find that only if the sphere sizes are different does the oscillatory reciprocal motion of the two spheres break the symmetry between extension and contraction during one swimming cycle. As a result, the swimmer moves in the direction of the smaller sphere. This is consistent with a recent work by Datt *et al.*,[39] who captured the effect of small deformations using the reciprocal theorem, whereas the current work allows arbitrary deformations. Our analytic approach allows us to go through the complexity of non-Newtonian fluids and understand how viscoelasticity enables breaking the symmetry of the swimming stroke. We show the time courses of the forces experienced by both spheres over a complete cycle and demarcate the viscoelastic contribution. The force needed to expand the swimmer is enhanced, whereas contraction requires less force compared to the Newtonian fluid. As a result, a swimmer with spheres of different sizes covers a larger distance during expansion and a smaller distance during contraction, which yields a net displacement. The size difference of the spheres, or more general the structural asymmetry of the swimmer, is an essential condition for locomotion and determines the direction of motion. This was also recognized by Pak *et al.*[35] for the "snowman" swimmer and Yasuda *et al.*[40] for the three-sphere swimmer in viscoelastic fluids. However, a further increase in the size ratio results in a situation where the larger sphere hardly moves and the smaller one oscillates about a mean position, so that the net displacement approaches zero. Thus, there exists an optimum size ratio that depends on the swimmer length and oscillation amplitude.

Another interesting feature is that the average flow field of such a reciprocal swimmer in a viscoelastic fluid is the one of a contractile force dipole ($1/r^2$), which is of longer range compared to linked-sphere swimmers in Newtonian fluids ($1/r^3$).[12,43,50] This is due to the fact that in leading order viscoelasticity contributes a contractile force-dipole flow field besides the conventional Newtonian Stokeslet to the flow field of each sphere.[42] A qualitatively similar feature has recently been reported for the two-sphere swimmer by Dombrowski *et al.*[51] In their work, instead of viscoelasticity, weak inertia induces directed motion toward the smaller sphere and they also observe a time-averaged flow field of a contractile force-dipole, which they term as "steady streaming." Thus, self-propulsion and long-range steady streaming can occur in systems with reciprocal deformations beyond the validity of the Stokes equations either due to inertia, viscoelasticity, shear-thinning/thickening, or anisotropic stresses in liquid crystals.[52,53] Future works could extend the current approach to account for these properties that are observed in biological fluids and biofilms.

Since Purcell formulated his famous scallop theorem, it is clear that microswimmers need to perform non-reciprocal periodic shape changes to move forward in a Newtonian fluid at low Reynolds numbers.[4] Using an oscillatory swimmer, we show explicitly that this no longer holds in a viscoelastic fluid, which typically occurs in biological systems. So, our work helps to explore principal features for swimming in viscoelastic fluids and through a multipole expansion establishes the swimming type of the oscillatory swimmer. We are not aware of any biological swimmer, which uses a reciprocal stroke pattern. However, our work encourages to perform further studies on reciprocal shape changes and search for biological swimmers that use them. In addition, our studies might also provide guidelines for designing novel artificial microswimmers to explicitly move in a viscoelastic environment.

ACKNOWLEDGMENTS

A.C. thanks the Humboldt foundation for financial support through a fellowship.

AUTHOR DECLARATIONS

Conflict of Interest

The authors have no conflicts to disclose.

Author Contributions

Marcel Eberhard: Conceptualization (supporting); Formal analysis (equal); Investigation (equal); Methodology (equal); Validation (equal); Writing – original draft (equal); Writing – review & editing (supporting). **Akash Choudhary:** Conceptualization (lead); Supervision (equal); Writing – original draft (equal); Writing – review & editing (supporting). **Holger Stark:** Supervision (equal); Writing – review & editing (lead).

DATA AVAILABILITY

The data that support the findings of this study are available within the article.

REFERENCES

[1]E. Lauga and T. R. Powers, "The hydrodynamics of swimming microorganisms," Rep. Prog. Phys. **72**, 096601 (2009).
[2]J. Elgeti, R. G. Winkler, and G. Gompper, "Physics of microswimmers-single particle motion and collective behavior: A review," Rep. Prog. Phys. **78**, 056601 (2015).
[3]A. Zöttl and H. Stark, "Emergent behavior in active colloids," J. Phys.: Condens. Matter **28**, 253001 (2016).
[4]E. M. Purcell, "Life at low Reynolds number," Am. J. Phys. **45**, 3–11 (1977).
[5]H. C. Berg, *E. coli in Motion (Biological and Medical Physics, Biomedical Engineering)* (Springer, 2003).
[6]H. Wada and R. R. Netz, "Hydrodynamics of helical-shaped bacterial motility," Phys. Rev. E **80**, 021921 (2009).
[7]K. Drescher, R. E. Goldstein, N. Michel, M. Polin, and I. Tuval, "Direct measurement of the flow field around swimming microorganisms," Phys. Rev. Lett. **105**, 168101 (2010).
[8]S. B. Babu and H. Stark, "Modeling the locomotion of the African trypanosome using multi-particle collision dynamics," New J. Phys. **14**, 085012 (2012).
[9]R. Vogel and H. Stark, "Rotation-induced polymorphic transitions in bacterial flagella," Phys. Rev. Lett. **110**, 158104 (2013).
[10]R. Dreyfus, J. Baudry, M. L. Roper, M. Fermigier, H. A. Stone, and J. Bibette, "Microscopic artificial swimmers," Nature **437**, 862–865 (2005).
[11]E. Gauger and H. Stark, "Numerical study of a microscopic artificial swimmer," Phys. Rev. E **74**, 021907 (2006).
[12]A. Najafi and R. Golestanian, "Simple swimmer at low Reynolds number: Three linked spheres," Phys. Rev. E **69**, 062901 (2004).
[13]J. E. Avron, O. Kenneth, and D. H. Oaknin, "Pushmepullyou: An efficient micro-swimmer," New J. Phys. **7**, 234 (2005).
[14]F. Alouges, A. DeSimone, and A. Lefebvre, "Optimal strokes for axisymmetric microswimmers," Eur. Phys. J. E **28**, 279–284 (2009).
[15]A. Montino and A. DeSimone, "Three-sphere low-Reynolds-number swimmer with a passive elastic arm," Eur. Phys. J. E **38**, 42 (2015).
[16]S. Suarez and A. A. Pacey, "Sperm transport in the female reproductive tract," Hum. Reprod. Update **12**, 23–37 (2006).
[17]R. Levy, D. B. Hill, M. G. Forest, and J. B. Grotberg, "Pulmonary fluid flow challenges for experimental and mathematical modeling," Integr. Comp. Biol. **54**, 985–1000 (2014).
[18]J. N. Wilking, T. E. Angelini, A. Seminara, M. P. Brenner, and D. A. Weitz, "Biofilms as complex fluids," MRS Bull. **36**, 385–391 (2011).
[19]A. Zöttl and H. Stark, "Modeling active colloids: From active Brownian particles to hydrodynamic and chemical fields," Annu. Rev. Condens. Matter Phys. **14**, 109 (2023).
[20]S. J. Ebbens and J. R. Howse, "In pursuit of propulsion at the nanoscale," Soft Matter **6**, 726 (2010).
[21]J. Wang, "Can man-made nanomachines compete with nature biomotors?," ACS Nano **3**, 4–9 (2009).
[22]E. Lauga, "Propulsion in a viscoelastic fluid," Phys. Fluids **19**, 083104 (2007).
[23]X. N. Shen and P. E. Arratia, "Undulatory swimming in viscoelastic fluids," Phys. Rev. Lett. **106**, 208101 (2011).
[24]M. P. Curtis and E. A. Gaffney, "Three-sphere swimmer in a nonlinear viscoelastic medium," Phys. Rev. E **87**, 043006 (2013).
[25]L. Zhu, E. Lauga, and L. Brandt, "Self-propulsion in viscoelastic fluids: Pushers vs. pullers," Phys. Fluids **24**, 051902 (2012).
[26]G. Li and A. M. Ardekani, "Undulatory swimming in non-Newtonian fluids," J. Fluid Mech. **784**, R4 (2015).
[27]S. Sahoo, S. P. Singh, and S. Thakur, "Role of viscoelasticity on the dynamics and aggregation of chemically active sphere-dimers," Phys. Fluids **33**, 017120 (2021).
[28]A. Zöttl and J. M. Yeomans, "Enhanced bacterial swimming speeds in macromolecular polymer solutions," Nat. Phys. **15**, 554–558 (2019).
[29]Y.-G. Irilan and F. R. Cunha, "Experimental and theoretical studies of the fluid elasticity on the motion of macroscopic models of active helical swimmers," Phys. Fluids **34**, 053103 (2022).
[30]P. E. Arratia, "Life in complex fluids: Swimming in polymers," Phys. Rev. Fluids **7**, 110515 (2022).
[31]G. Li, E. Lauga, and A. M. Ardekani, "Microswimming in viscoelastic fluids," J. Non-Newtonian Fluid Mech. **297**, 104655 (2021).
[32]E. Lauga, "Locomotion in complex fluids: Integral theorems," Phys. Fluids **26**, 081902 (2014).
[33]T. Qiu, T.-C. Lee, A. G. Mark, K. I. Morozov, R. Münster, O. Mierka, S. Turek, A. M. Leshansky, and P. Fischer, "Swimming by reciprocal motion at low Reynolds number," Nat. Commun. **5**, 5119 (2014).
[34]K. Han, C. W. Shields IV, B. Bharti, P. E. Arratia, and O. D. Velev, "Active reversible swimming of magnetically assembled 'microscallops' in non-Newtonian fluids," Langmuir **36**, 7148–7154 (2020).
[35]O. S. Pak, L. Zhu, L. Brandt, and E. Lauga, "Micropropulsion and microrheology in complex fluids via symmetry breaking," Phys. Fluids **24**, 103102 (2012).
[36]J. A. Puente-Velázquez, F. A. Godínez, E. Lauga, and R. Zenit, "Viscoelastic propulsion of a rotating dumbbell," Microfluid. Nanofluid. **23**, 108 (2019).
[37]J. P. Binagia and E. S. Shaqfeh, "Self-propulsion of a freely suspended swimmer by a swirling tail in a viscoelastic fluid," Phys. Rev. Fluids **6**, 053301 (2021).
[38]L. Kroo, J. P. Binagia, N. Eckman, M. Prakash, and E. S. Shaqfeh, "A freely suspended robotic swimmer propelled by viscoelastic normal stresses," J. Fluid Mech. **944**, A20 (2022).
[39]C. Datt, B. Nasouri, and G. J. Elfring, "Two-sphere swimmers in viscoelastic fluids," Phys. Rev. Fluids **3**, 123301 (2018).
[40]K. Yasuda, M. Kuroda, and S. Komura, "Reciprocal microswimmers in a viscoelastic fluid," Phys. Fluids **32**, 093102 (2020).
[41]N. C. Keim, M. Garcia, and P. E. Arratia, "Fluid elasticity can enable propulsion at low Reynolds number," Phys. Fluids **24**, 081703 (2012).
[42]K. D. Housiadas and R. I. Tanner, "A high-order perturbation solution for the steady sedimentation of a sphere in a viscoelastic fluid," J. Non-Newtonian Fluid Mech. **233**, 166–180 (2016).
[43]G. P. Alexander, C. M. Pooley, and J. M. Yeomans, "Hydrodynamics of linked sphere model swimmers," J. Phys.: Condens. Matter **21**, 204108 (2009).
[44]The flow field $\boldsymbol{u}_n$ is also valid for oscillating spheres as long as $\mathrm{De} = \lambda\omega \ll 1$ meaning the polymer relaxation in the viscoelastic fluid is fast compared to the swimmer oscillations. Typical numbers, which justify this choice, are $\lambda \leq 10^{-2} - 10^{-1}\mathrm{s}$ for dilute polymer solutions and $\omega \sim 1\mathrm{s}^{-1}$. In addition to the zeroth-order term of the flow field, where one makes the typical assumption that vorticity diffusion time is sufficiently small, one can show that the first-order term obeys the Stokes equation with an inhomogeneity that depends on the zeroth-order term of $\boldsymbol{u}_n$. Thus, it is independent of time, and a quasistatic approximation holds. A typical estimate for the vorticity diffusion time is $a^2/\nu \approx 10^{-6}\mathrm{s}$ with $a = 1\mu\mathrm{m}$ and $\nu = 10^{-6}\mathrm{m}^2/\mathrm{s}$.
[45]C. W. Oseen, *Neuere Methoden Und Ergebnisse in Der Hydrodynamik* (Akademische Verlagsgesellschaft MBH, 1927), Vol. 1.
[46]J. Happel and H. Brenner, *Low Reynolds Number Hydrodynamics: With Special Applications to Particulate Media* (Springer Science & Business Media, 1983), Vol. 1.
[47]R. Golestanian and A. Ajdari, "Analytic results for the three-sphere swimmer at low Reynolds number," Phys. Rev. E **77**, 036308 (2008).
[48]M. J. Lighthill, "On the squirming motion of nearly spherical deformable bodies through liquids at very small Reynolds numbers," Commun. Pure Appl. Math. **5**, 109–118 (1952).
[49]Note that we neglect here a term linear in De, which would arise from the coupling of the flow fields from the two individual spheres. For $L \gg a$ it is negligible against the contributions from the single spheres, when calculating the first-order term of the total flow field.
[50]C. M. Pooley, G. P. Alexander, and J. M. Yeomans, "Hydrodynamic interaction between two swimmers at low Reynolds number," Phys. Rev. Lett. **99**, 228103 (2007).

[51]T. Dombrowski, S. K. Jones, G. Katsikis, A. P. S. Bhalla, B. E. Griffith, and D. Klotsa, "Transition in swimming direction in a model self-propelled inertial swimmer," Phys. Rev. Fluids **4**, 021101 (2019).
[52]P. R. Secor, L. K. Jennings, L. A. Michaels, J. M. Sweere, P. K. Singh, W. C. Parks, and P. L. Bollyky, "Biofilm assembly becomes crystal clear–filamentous bacteriophage organize the *Pseudomonas aeruginosa* biofilm matrix into a liquid crystal," Microbial Cell **3**, 49 (2016).
[53]Y. I. Yaman, E. Demir, R. Vetter, and A. Kocabas, "Emergence of active nematics in chaining bacterial biofilms," Nat. Commun. **10**, 2285 (2019).